Interdomain Communication between Weak Structural Elements within a Disease-Related Human tRNA†

Marc D. Roy, Lisa M. Wittenhagen, Brian E. Vozzella, and Shana O. Kelley*

Boston College, Eugene F. Merkert Chemistry Center, Chestnut Hill, Massachusetts 02467

Received September 22, 2003; Revised Manuscript Received November 8, 2003

ABSTRACT: The structure of the human mitochondrial (hs mt) tRNA$^{Leu(UUR)}$ features several domains that are predicted to exhibit limited thermodynamic stability. An elevated frequency of disease-related mutations within these domains suggests a link between structural instability and the functional effects of pathogenic mutations. A series of tRNAs featuring mutations within the D and anticodon stems were prepared and investigated using nuclease probing. Structural mapping studies indicated that these domains were partially denatured for the wild type (WT) hs mt tRNA$^{Leu(UUR)}$ and were significantly stabilized by mutations introducing additional or stronger base pairs into the stem regions. In addition, trends in the aminoacylation activities of the D stem mutants suggested that the loose structure is required for function, with mutants displaying the most ordered structures exhibiting the lowest levels of aminoacylation activity. A pronounced interdependence of the structures of the anticodon and D stems was observed, with mutations strengthening the D stem stabilizing the anticodon stem and vice versa. The existence of strong interdomain communication was further elucidated with a mutant of hs mt tRNA$^{Leu(UUR)}$ containing a stabilized D stem and a pathogenic mutation that disrupted the anticodon stem. Strengthening the structure of the D stem completely restored the function of the disease-related mutant to WT levels, indicating that propagated structural weaknesses contribute to the functional deactivation of this tRNA by mutations.

tRNAs[1] are essential components of the protein synthesis machinery (*1*). Translation of genetic information into protein sequences requires the delivery of amino acids to the ribosome by tRNAs; thus, the efficiency and fidelity of protein synthesis rely on the presence of functional tRNAs within the cell. Over the past decade, a number of diseases correlated with mutations in hs mt tRNA genes have been discovered (*2*, *3*). The deleterious effects of the mutations on hs mt tRNA structure and function may underlie the resultant disease states (*4*, *5*).

The primary sequences and secondary structures of hs mt tRNAs are significantly different from those of canonical bacterial and cytoplasmic tRNAs (*6*), and the three-dimensional structures remain uncharacterized at the molecular level. Hs mt tRNAs typically have shortened sequences relative to other tRNAs, ranging from 62 to 78 nucleotides in length, and contain 33−75% AU base pairs (*7*); bacterial analogues are 74−95 nucleotides in length and contain a lower percentage of AU base pairs, typically 11−38% (*8*). Truncations within the D and TψC domains are also common in hs mt tRNAs (*6*). Highly conserved nucleotides present in canonical tRNAs are often absent within mitochondrial analogues, altering the pattern of tertiary interactions that are tightly conserved in nonmitochondrial sequences. Therefore, while hs mt tRNAs must adopt an L-shaped structure typical of canonical tRNAs in order to function in ribosomal protein synthesis, their folded structures may be constructed with a different set of intramolecular contacts. Additionally, because of their shortened and AU-rich sequences, hs mt tRNAs are predicted to have low thermodynamic stabilities (*6*). The divergence from the common canonical structure may heighten the susceptibility of mitochondrial tRNAs toward conformational defects caused by pathogenic point mutations.

Hs mt tRNA$^{Leu(UUR)}$ is a particularly interesting case with 20 documented pathogenic mutations (Figure 1) (*9*). Several of the disease-related mutations within hs mt tRNA$^{Leu(UUR)}$ have been investigated at the cellular and molecular level, and varied functional defects have been observed (*10*−*17*). Limited direct experimental evidence concerning the structure of this tRNA or disease-related mutants is available.

The predicted base-pairing pattern for hs mt tRNA$^{Leu(UUR)}$ closely resembles the canonical cloverleaf tRNA structure (*18*). Of the nine long-range tertiary interactions that are characteristic of most tRNAs, hs mt tRNA$^{Leu(UUR)}$ retains eight, with the exception being the 9-(23-12) tertiary interaction that is lost due to an A−C mispair within the D stem (*6*). In contrast to the majority of hs mt tRNAs that commonly retain only the "core" interactions between the D stem and the variable loop, hs mt tRNA$^{Leu(UUR)}$ should maintain a stable tertiary structure.

† Financial support of this project is provided by the National Institutes of Health (R01 GM063890-01A2), the Dreyfus Foundation, and the Research Corporation. S.O.K. acknowledges a Dreyfus New Faculty Award and a Research Innovation Award that provided support for this work.

* To whom correspondence should be addressed. Tel: 617-552-3121. Fax: 617-552-2705. E-mail: shana.kelley@bc.edu.

[1] Abbreviations: hs mt, human mitochondrial; tRNA, transfer ribonucleic acid; PAGE, polyacrylamide gel electrophoresis; D, dihydrouridine; DEPC, diethyl pyrocarbonate; WT, wild type; DST, D stem transplant; MELAS, mitochondrial myopathy, encephalopathy, lactic acidosis, and strokelike episodes; MIDD, maternally inherited diabetes and deafness.

10.1021/bi035711z CCC: $27.50
Published on Web 12/20/2003

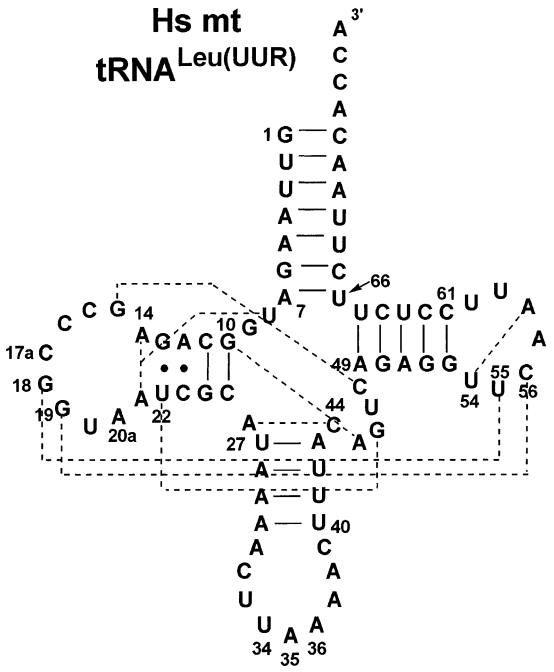

FIGURE 1: Predicted secondary structure of hs mt tRNA$^{Leu(UUR)}$. Expected tertiary interactions are indicated with dotted lines. Numbers represent positions as determined by the canonical tRNA numbering system (*19*).

While the hs mt tRNA$^{Leu(UUR)}$ features conserved nucleotides that would permit the formation of a structure analogous to canonical tRNAs (Figure 1) (*19*), a unique characteristic of this tRNA is the presence of a thermodynamically unstable anticodon stem comprised of four A−U pairs, rather than the five base pairs typically observed. Another striking feature within the structure is a destabilized D stem, which contains only two Watson−Crick pairs, one A−C mispair, and one G−U pair adjacent to the D loop. Mispairs are commonly present adjacent to the D or TΨC loop in mt tRNAs (*6*). However, this feature is believed to offset the shorter, sterically hindered loops of mt tRNAs, which are relieved of strain when flanked by a mispair (*6*). The presence of a G−U pair at this position in hs mt tRNA$^{Leu(UUR)}$ does not appear to be necessary for the mitigation of loop strain, as the D loop in this tRNA contains 10 bases as opposed to the canonical eight (*7*, *19*).

In the present study, we investigate the structural properties of hs mt tRNA$^{Leu(UUR)}$ (Figure 1) with a particular focus on domains within this molecule that appear unstable. The D stem and anticodon stem of hs mt tRNA$^{Leu(UUR)}$ are destabilized by the low number of hydrogen bonds preserving structural integrity. By preparing a series of mutants that feature alterations to these domains, the role of individual base pairs in the structure and function of this tRNA could be probed. These studies indicate that the hs mt tRNA$^{Leu(UUR)}$ does possess a fragile structure that renders it vulnerable to the effects of disease-related mutations. However, the destabilizing features of this particular tRNA appear to be essential for proper function.

EXPERIMENTAL SECTION

Preparation of tRNA Constructs. Plasmid DNA templates for in vitro transcription were created as described (*10*, *11*). Plasmids were harvested from *Escherichia coli* DH5α in milligram quantities and digested with *Mva*1 (Ambion) to generate the 3′-CCA end. The digested plasmids were phenol/chloroform extracted (pH 8), ethanol precipitated, resuspended in water, and further purified using G-25 columns (Amersham Pharmacia). In vitro transcription reactions contained template DNA (200−400 μg in 1 mL), T7 RNA polymerase (overexpressed in *E. coli*), RNasin (400 units/mL, Promega), 40 mM Tris-HCl (pH 8), 10 mM NaCl, 2 mM spermidine, 20 mM $MgCl_2$, 4 mM NTPs, and 5 mM dithiothreitol. Transcription reactions were incubated for 6 h at 37 °C, with the addition of a second aliquot of polymerase after 3 h. Plasmid DNA was digested with DNase I (60 units/mL, Takara). Transcription products were extracted with 5:1 phenol (pH 4.7)/chloroform and ethanol precipitated. The hs mt tRNA$^{Leu(CUN)}$ does not possess a 5′-G; therefore, this tRNA has a decreased transcription efficiency; sufficient tRNA was obtained with a 5 mL transcription sample that was desalted with NAP-25 columns (Amersham Pharmacia) before precipitation. Samples were purified by 12% denaturing PAGE using a 0.5X TBE buffer (45 mM Tris base/45 mM boric acid/1 mM EDTA) on a 26 cm × 16.5 cm × 3 mm gel for 4 h. tRNA transcripts were recovered by electroelution, ethanol precipitated, and resuspended in 0.5X TE (5 mM Tris-HCl (pH 8), 0.5 mM EDTA). All solutions were prepared with DEPC-treated water.

Concentrations of tRNA solutions were determined by quantitating the absorbance at 260 nm and applying an extinction coefficient of 895 000 M^{-1} (mononucleotide) cm^{-1} (*20*). tRNA samples were annealed with incubation at 70 °C for 5 min in 0.5X TE followed by addition of $MgCl_2$ (10 mM) and immediate cooling on ice.

Preparation of 5′-[^{32}P]-Labeled hs mt tRNA$^{Leu(UUR)}$. tRNA samples were 5′-dephosphorylated using calf intestinal alkaline phosphatase (Takara). Dephosphorylated tRNAs (100 pmols) were 5′-radiolabeled in reactions containing 100 pmol of γ-^{32}P-ATP (ICN Biomedicals, 7000 Ci/mmol), 100 units of T4 polynucleotide kinase (New England Biolabs), 70 mM Tris-HCl (pH 7.6), 10 mM $MgCl_2$, and 5 mM dithiothreitol, The labeling reactions were carried out for 30 min at 37 °C and purified using G-25 columns. Labeled samples were further purified using 12% denaturing PAGE with a 0.5X TBE buffer, electroeluted, and ethanol precipitated. Samples were resuspended in 0.5X TE buffer.

Enzymatic Probing. Experiments were conducted under nondenaturing conditions in a total reaction volume of 20 μL containing 40 mM Tris-HCl (pH 7.5), 40 mM NaCl, 10 mM $MgCl_2$, and 1 mM spermine (1 mM $ZnCl_2$ was also added to nuclease S1 digests) (*12*). The radiolabeled samples (2×10^4 cpm) were supplemented with cold tRNA at a concentration of 0.05 μg/μL and annealed by heating in 40 mM Tris-Cl (pH 7.5) at 70 °C for 5 min, followed by the addition of NaCl, $MgCl_2$, spermine, and $ZnCl_2$ (when applicable). Annealed samples were cooled on ice for 20 min.

Nuclease probing experiments were performed using 25, 6×10^{-2}, and 1.75×10^{-3} U of nuclease S1 (Fermentas), ribonuclease T2 (Sigma), and ribonuclease V1 (Ambion), respectively. Reactions were carried out at 25 °C for 5 min and halted by the addition of 5 μL of denaturing PAGE loading buffer (8 M urea/45 mM Tris base/45 mM boric acid/1 mM EDTA).

Sequencing Reactions. A guanine ladder was created using ribonuclease T1 (Fermentas). Labeled WT hs mt $tRNA^{Leu(UUR)}$ (2×10^4 cpm) supplemented with cold tRNA at a concentration of 0.1 μg/μL in 50 mM Tris base and 2 mM EDTA was incubated at 70 °C for 5 min and cooled on ice (*21*). RNase T1 (0.02 U) was added to the 5 μL reaction solution, which was incubated at 37 °C for 20 min. An alkaline ladder was also prepared with WT hs mt $tRNA^{Leu(UUR)}$ in 10 mM $NaHCO_3$ and 2 mM EDTA (5 μL). The sample mixtures were heated for 8 min at 90 °C (*21*). Each reaction was stopped through the addition of 5 μL of denaturing PAGE loading buffer followed by cooling on ice.

Gel Electrophoresis Analysis of tRNA Reactions. Probing reactions were analyzed on 21 cm (w) × 40 cm (h) × 0.4 mm (d) 20% denaturing PAGEs buffered with 0.5X TBE. Gels were typically electrophoresed for 1.25 h at 25 mA and then exposed to a Kodak K-plate for 2 h. Imaging was performed with a Bio-Rad Molecular Imager FX Pro Plus phosphoimager.

Preparation of hs mt LeuRS. Hs mt LeuRS was cloned and purified as described (*10*, *22*). A fresh transformation from the cloned DNA was used for each protein preparation. The purity of the protein was confirmed by SDS−PAGE, and its concentration was determined by Bradford assay.

Aminoacylation Assays. tRNAs were annealed immediately before aminoacylation assays as indicated above. Assays were performed at 37 °C in reaction mixtures containing 50 mM HEPES (pH 7.6), 100 μM spermine, 25 mM KCl, 0.2 mg/mL bovine serum albumin, 2.5 mM ATP, 100 μM leucine, 6 μM [3,4,5-^{3}H]leucine (173 Ci/mmol, Perkin-Elmer), 7 mM $MgCl_2$, 20 nM enzyme, and 3 μM tRNA. Results were analyzed as described (*23*).

Native Gel Electrophoresis. Samples containing tRNA were annealed as described above. A tRNA concentration of 1 μM was obtained with the addition of native loading buffer (*10*). Samples were analyzed by 10% native PAGE in 0.5X TB buffer [45 mM Tris (pH 7.5) and 45 mM boric acid]. Gels were stained by ethidium bromide and visualized using an Epi Chemi II Darkroom (UVP Imaging).

Thermal Denaturation Measurements. Quartz cuvettes were pretreated with DEPC water. In vitro transcribed $tRNA^{Leu(UUR)}$ (0.38 μM) samples were annealed as described above. Annealed tRNAs were analyzed in a buffer containing 50 mM sodium cacodylate (pH 7), 10 mM $MgCl_2$, and 600 mM NaCl. The change in absorbance for each sample was measured at 260 nm on an AVIV spectrophotometer (model 14DS UV/vis) from 25 to 95 °C at 1 °C/min. Melting temperatures were obtained from the maxima of the first derivative of the thermal denaturation curves.

RESULTS AND DISCUSSION

Solution Structure of WT hs mt $tRNA^{Leu(UUR)}$. The solution structure of the WT $tRNA^{Leu(UUR)}$ was probed using a series of nucleases. The goal of these experiments was to assess the overall structure of this tRNA and to probe the integrity of domains (e.g., the anticodon and D stems) that are predicted to exhibit marginal thermodynamic stability based on the low numbers of hydrogen bonds present within the structures. Given that the hs mt $tRNA^{Leu(UUR)}$ contains many of the nucleotides expected to form the tertiary interactions typically stabilizing the L-shaped fold characteristic of tRNAs (Figure 1), a structure similar to that observed for tRNAs previously characterized by X-ray crystallography was anticipated (*24*−*26*). However, the unstable stems of the hs mt $tRNA^{Leu(UUR)}$ would be expected to introduce conformational lability and could alter the overall fold.

Nuclease S1 and RNase T2 were used to define single-stranded or loosely structured regions of hs mt $tRNA^{Leu(UUR)}$ (Figure 2). Interestingly, two regions that exhibited significant accessibility to S1 and T2 were the D and anticodon stems. Within the D stem, A12 appeared particularly susceptible to the nucleases, especially RNase T2. The nucleotide expected to pair with A12 based on the predicted secondary structure (Figure 1), C23, also exhibited high accessibility. Other nucleotides within the D stem, including G10, U22, and G24, were also cleaved by nuclease S1.

Nucleotides within the anticodon stem also exhibited high levels of cleavage with both nucleases specific for single-stranded structures. Nuclease S1 exhibited high reactivity with U27−A31, and RNase T2 efficiently cleaved A28−A31. Surprisingly, the accessibility of these positions appeared more pronounced than for the anticodon nucleotides. Cleavage at U26−A28 is also observed with RNase V1, which recognizes structured or double-stranded regions (see Supporting Information). The observation of cleavage by this nuclease along with those that recognize single-stranded structures indicates that different conformations of this stem may exist or that dynamic denaturation of the double-stranded form permits capture by the single-stranded nucleases.

These experiments indicated that the structure of hs mt $tRNA^{Leu(UUR)}$ contained several regions that despite the predicted secondary structure were at least transiently unduplexed. However, the observation of the highest level of D stem cleavage with RNase T2 at the A12−C23 pair, which would be predicted to be the weakest part of this domain, suggests that the proposed structure is likely an accurate representation of the overall fold and that the stem is not completely denatured, as suggested in a prior structural analysis of this tRNA (*12*). The weak hydrogen-bonding patterns within the D stem of hs mt $tRNA^{Leu(UUR)}$ appear insufficient for the preservation of a rigid helical structure. Likewise, the high AU content of the anticodon stem renders this region weak and prone to denaturation. However, the structure of hs mt $tRNA^{Leu(UUR)}$ must be sufficiently robust for function; it is possible that the presence of modified bases in the native tRNA introduces further stabilization that cannot be monitored in this system.

Interestingly, 14 out of the 20 disease-related mutations discovered within the hs mt $tRNA^{Leu(UUR)}$ are located within the D and anticodon domains (*9*). The pronounced structural weaknesses within these regions of the tRNA may augment the response of this biomolecule to the presence of point mutations. The D and anticodon stems appear only marginally stable and therefore may not be able to retain a folded conformation when destabilizing sequence changes are introduced.

Manipulation of the Structure of the hs mt $tRNA^{Leu(UUR)}$ D Stem. The nuclease probing experiments revealed patterns of cleavage that were consistent with a defined three-dimensional fold but with several domains within the canonical cloverleaf structure exhibiting significant lability. A series of tRNA mutants were constructed to probe how

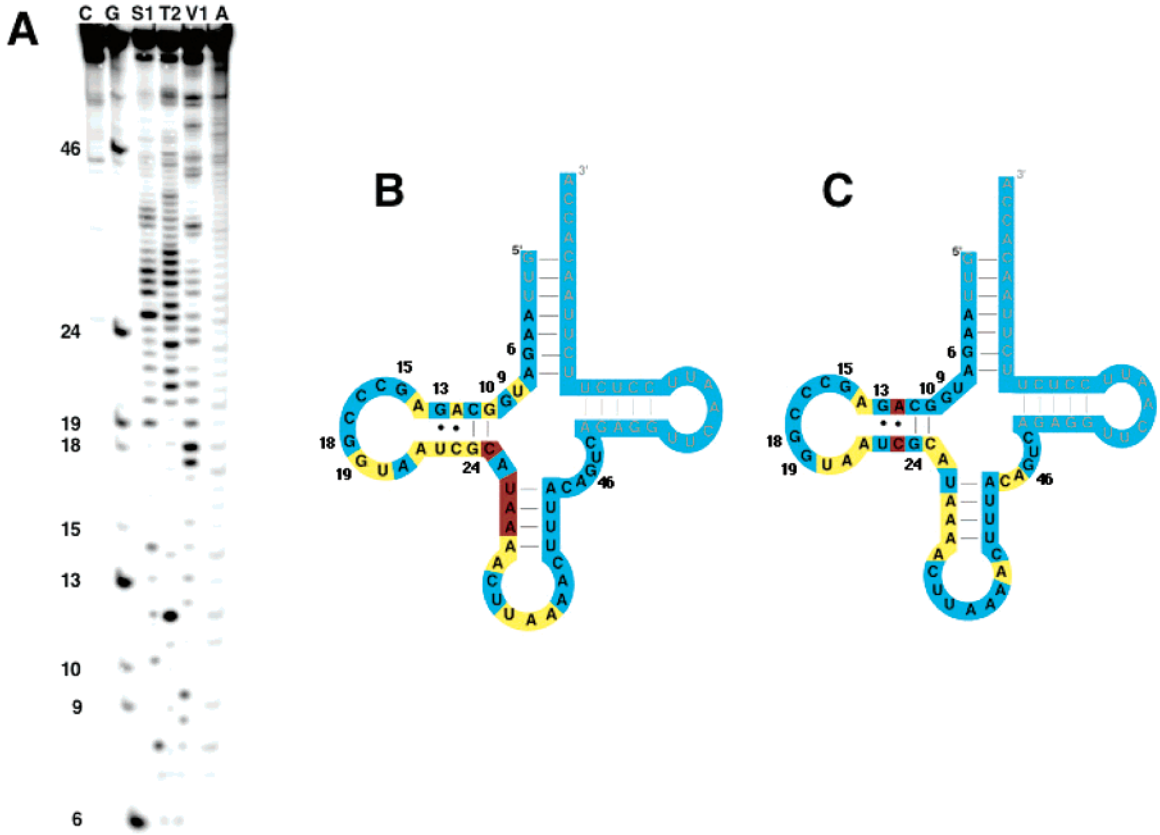

FIGURE 2: Enzymatic probing of WT hs mt tRNA$^{Leu(UUR)}$. (A) 5′-^{32}P-labeled tRNA was subjected to cleavage with nuclease S1, RNase T2, or RNase V1 and analyzed using 20% denaturing PAGE alongside unreacted control tRNA (C), a denatured RNase T1 ladder (G), and an alkaline ladder (A). (B) Schematic depiction of cleavage data for nuclease S1. Nucleotides shaded red were highly accessible to the nuclease, while those shaded yellow were moderately accessibly and those shaded blue exhibited low accessibility. Nucleotides shown in gray could not be visualized in this experiment. (C) Schematic depiction of cleavage data for RNase T2. The color scheme is the same as in panel B.

stabilizing mutations changed the structure of these regions. In addition, the interplay between the unique structural features of this tRNA and its function was addressed through experiments monitoring the aminoacylation activity of stabilized mutants (Figure 4).

The D stem of hs mt tRNA$^{Leu(UUR)}$ contains two GC pairs, a CA pair and a GU pair. The latter base pair is highly conserved particularly among mammals (*7*), while the former pair only appears in *H. sapiens*, *P. paniscus*, and *G. gorilla* and is commonly an UA pair in most other higher and lower eukaryotes (*7*). To assess how the non-Watson−Crick pairs found within this stem affected the structure and function of hs mt tRNA$^{Leu(UUR)}$, the hs mt tRNA$^{Leu(CUN)}$ isoacceptor (Figure 3A) and the following series of hs mt tRNA$^{Leu(UUR)}$ mutants (Figure 3B) were prepared as follows: an A12G mutant featuring a G12:C23 pair, a C23U mutant featuring a A12:U23 pair, an U22C mutant featuring a G13:C22 pair, and a construct that featured the fully base-paired D stem of the hs mt tRNA$^{Leu(CUN)}$ structure (DST). The hs mt tRNA$^{Leu(CUN)}$ does not contain the destabilizing features of the UUR isoacceptor (*18*), but both tRNAs are aminoacylated at similar levels (Figure 4A). Therefore, introducing the tRNA$^{Leu(CUN)}$ D stem into the tRNA$^{Leu(UUR)}$ structure might provide insight into why the unstable stem found in the latter tRNA is present.

This series of mutants exhibited similar mobilities when analyzed by native gel electrophoresis, indicating that the global conformations of the tRNAs were similar (see Supporting Information) (*27*). In addition, measurement of the melting temperatures (see Supporting Information) revealed that the mutants exhibited similar thermal stabilities, with T_m values of 54.4 ± 0.2 (WT hs mt tRNA$^{Leu(UUR)}$), 53.8 ± 0.4 (A12G), 54.1 ± 0.1 (U22C), 54.2 ± 0.3 (C23U), 58.2 ± 0.1 (DST), and 55.2 ± 0.2 (WT hs mt tRNA$^{Leu(CUN)}$) °C. The only tRNA with a significantly elevated T_m was the DST tRNA (58 °C), which contains two additional Watson−Crick base pairs in the D stem that appear to introduce stability into the tRNA$^{Leu(UUR)}$ structure.

A comparison of nuclease probing studies using RNase T2 and nuclease S1 with the series of D stem mutants revealed interesting structural differences among the constructs (Figures 5 and 6). The C23U mutant displayed only a modest decrease in cleavage at A12 relative to the WT sequence, and no change in cleavage efficiencies was observed at the nucleotides adjacent to A12, indicating that the introduction of a Watson−Crick pair does not significantly alter the local structure of the D stem (Figures 5A and 6A). Less cleavage was observed at U23, confirming the presence of a more stable base pair at this mutated position. Interestingly, less cleavage was observed at nucleotides within the anticodon stem in the C23U mutant. It appears that stabilization resulting from the sequence change is propagated through the structure to this distal region.

The A12G mutant, with a GC pair in the 12:23 position, exhibits significantly reduced cleavage within the D stem as compared with the WT tRNA$^{Leu(UUR)}$ when incubated with either RNase T2 or nuclease S1 (Figures 5C and 6C). Changes in the reactivity of A14 for the A12G mutant

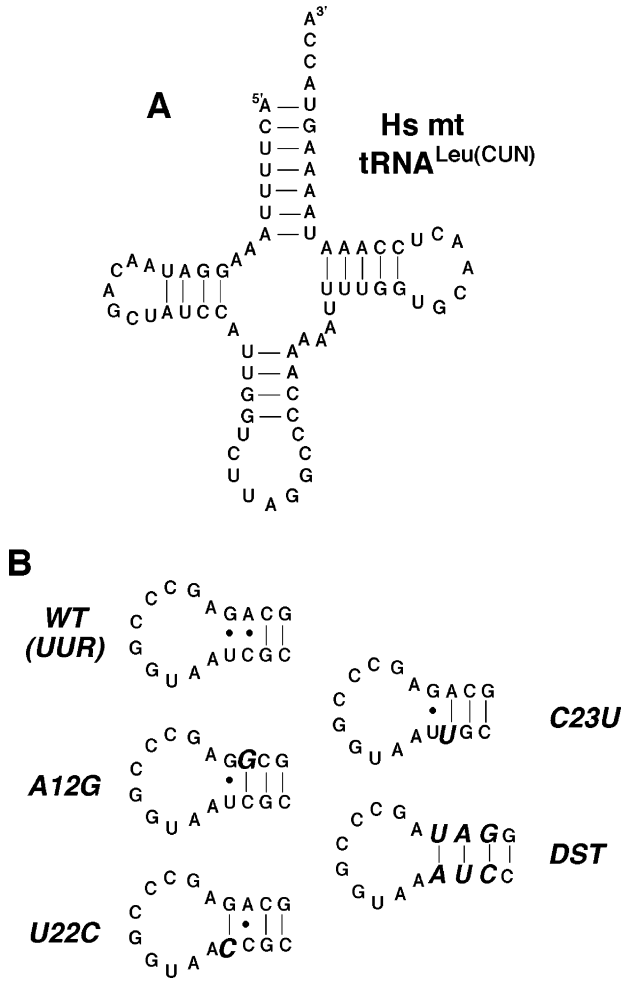

FIGURE 3: (A) Predicted secondary structure of hs mt tRNA$^{Leu(CUN)}$. (B) Hs mt tRNA$^{Leu(UUR)}$ constructs with stabilized D stems. Three point mutants (A12G, U22C, and C23U) and a construct featuring the D stem of the tRNA$^{Leu(CUN)}$ isoacceptor transplanted into the tRNA$^{Leu(UUR)}$ structure (DST) were generated to explore the effect of the structure of the D stem.

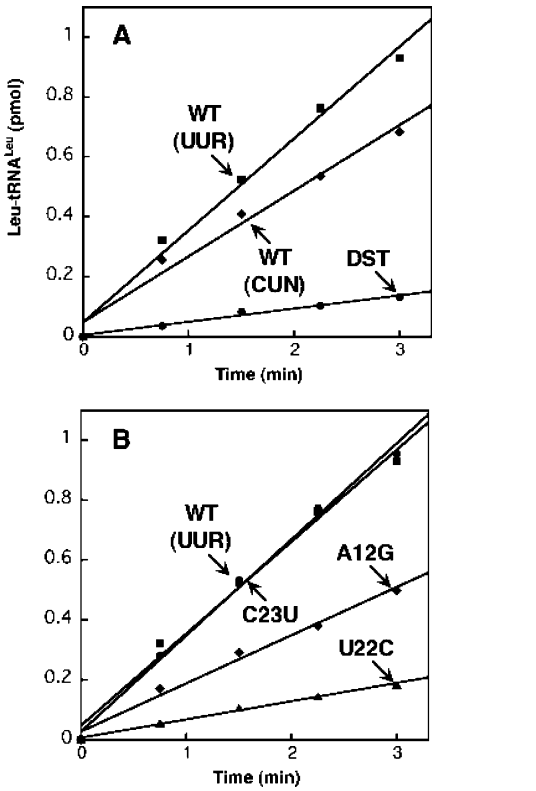

FIGURE 4: Aminoacylation of hs mt tRNA^{Leu} constructs. (A) Aminoacylation of WT hs mt tRNA$^{Leu(UUR)}$ (■), WT hs mt tRNA$^{Leu(CUN)}$ (♦), and DST (●) by hs mt LeuRS monitored at pH 7.6 at 37 °C with 3 μM tRNA and 20 nM LeuRS. (B) Aminoacylation of WT hs mt tRNA$^{Leu(UUR)}$ (■), C23U (●), A12G (♦), and U22C (▲) with conditions the same as in panel A. Data sets shown represent averages of multiple experimental trials; aminoacylation efficiencies observed for a given tRNA varied by less than 10% among independent experiments.

relative to the WT tRNA are also observed, with protection of this nucleotide observed with nuclease S1. The altered cleavage efficiency indicates that the orientation of this nucleotide, which participates in an important contact with U8 (*7*), is affected. As noted above for the C23U mutant, the anticodon stem nucleotides are significantly more protected in the presence of the stabilizing A12G mutation, reinforcing the idea that the introduction of additional hydrogen bonds into the D stem has a significant effect on the conformation of other parts of the structure.

The hs mt tRNA$^{Leu(UUR)}$ DST construct featuring the D stem of the hs mt tRNA$^{Leu(CUN)}$ isoacceptor also displayed decreased cleavage in the transplanted region with both single-stranded nucleases tested (Figures 5B and 6B). The accessibility of A14 also appears perturbed as noted for the A12G mutant, with both nucleases exhibiting lowered reactivity with this site. In fact, the cleavage at all of the D loop nucleotides is lower within this construct, indicating that the structure of this loop is influenced by the structure of the transplanted stem.

An U22C mutant was also examined to probe the influence of the terminal GU pair within the D stem (Figures 5D and 6D). Interestingly, the cleavage patterns for this mutant were almost identical to those obtained for the C23U mutant, indicating that the formation of the GC pair at the end of the stem had a similar effect as the introduction of the AU pair at the next position. Overall, the C23U mutant appears more structured and less accessible to nucleases binding unpaired nucleotides than the WT sequence.

Functional Properties of D Stem Mutants. A comparison of aminoacylation of the D stem mutants by the hs mt LeuRS revealed several interesting trends that connect the structure of the hs mt tRNA$^{Leu(UUR)}$ to its functional properties. Importantly, the introduction of point mutations into the D stem that introduced Watson−Crick base pairs did not increase the aminoacylation activity of the tRNA, indicating that an active fold is obtained even with the unstable stem (Figure 4B).

The aminoacylation efficiency for the C23U mutant, with an UA pair replacing the native CA pair, was indistinguishable from the WT sequence (Figure 4B). Most other higher eukaryotes have an UA pair at this position (*7*), so it is therefore not surprising that the mispair can be replaced with this Watson−Crick pair without affecting activity. The introduction of a GC pair (A12G) at the same position, however, decreased the reactivity by ∼50% (Figure 4B), indicating that the A-containing base pair is either an important structural modulator or a recognition determinant for hs mt LeuRS. The hs mt tRNA$^{Leu(UUR)}$ DST construct containing the tRNA$^{Leu(CUN)}$ D stem also displayed significantly reduced activity (Figure 4A). Thus, the sequence with

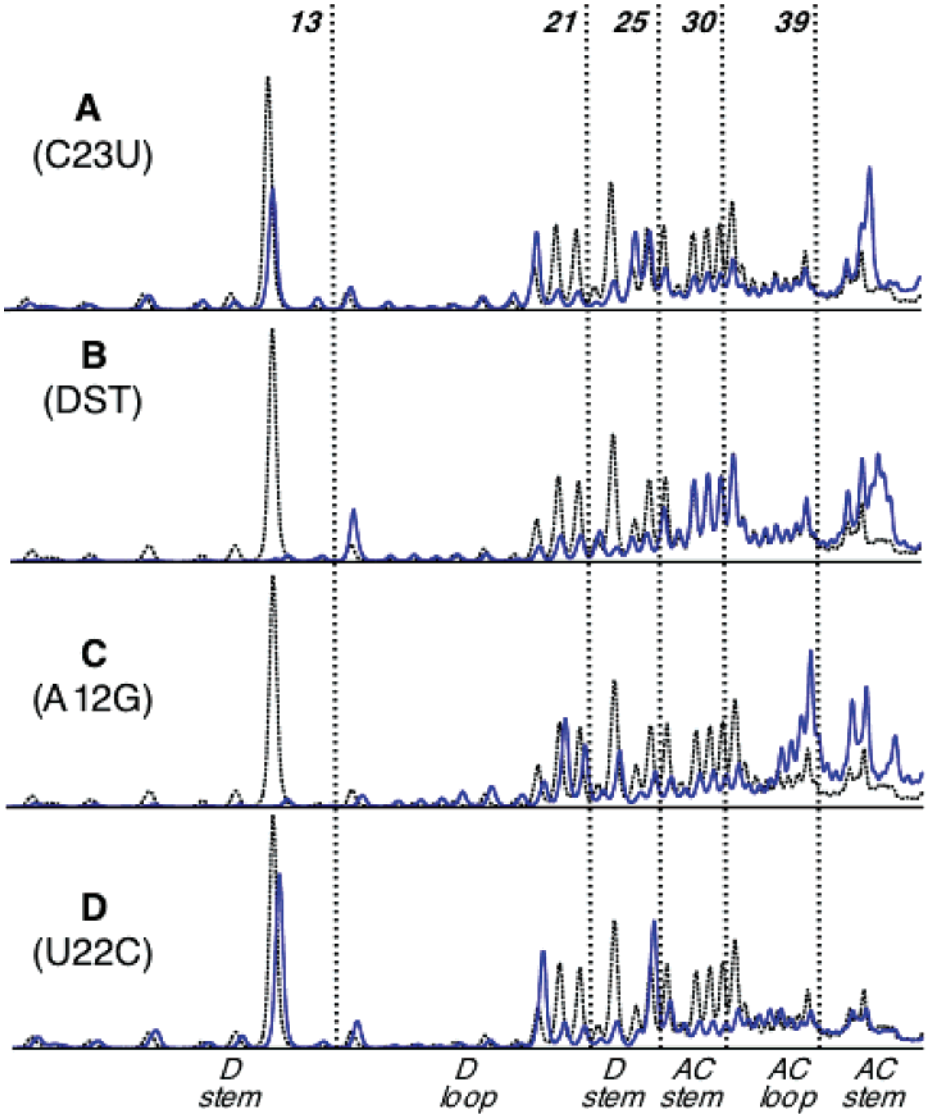

FIGURE 5: Enzymatic cleavage of WT hs mt $tRNA^{Leu(UUR)}$ and mutants. 5′-^{32}P-labeled tRNAs were subjected to enzymatic cleavage and analyzed using 20% denaturing PAGE (see Supporting Information for gel image). Data were generated through quantitating the cleavage along each sample lane. Histograms represent the normalized results of RNase T2 cleavage under native conditions. Hs mt $tRNA^{Leu(UUR)}$ native conditions. Probing results for hs mt $tRNA^{Leu(UUR)}$ mutants (colored) are compared to the WT sequence (dashed black). Histograms A, B, C, and D represent the comparison of WT probing data to that of mutants C23U, DST, A12G, and U22C, respectively. The data are divided into the four analyzed structural domains of the tRNA using dashed, vertical lines. The number to the left of each line is the position that terminates each domain.

more robust base pairing only produces a functional D stem when embedded within the CUN sequence.

The A12G and DST hs mt $tRNA^{Leu(UUR)}$ constructs contain stabilizing sequence changes that were reflected in the nuclease cleavage profiles obtained. Both of these mutants exhibited very low cleavage levels in the D stem and also exhibited changes in the accessibility of A14 (Figures 5B,C and 6B,C). These results may indicate that the increased stability of the D stem introduces subtle structural changes altering the conformation of the D domain and the arrangement of functional groups important for recognition by the cognate tRNA synthetase.

The U22C mutant also exhibited significantly lowered aminoacylation activity (Figure 4B). The introduction of a GC pair in the place of the terminal GU pair found within the WT sequence does appear to stabilize the structure, and the cleavage patterns observed for this mutant closely mirror those obtained with the C23U mutant (Figures 5A,D and 6A,D). The observation of similar structural properties but different aminoacylation efficiencies for the U22C and C23U mutants indicates that loss in activity for the former tRNA may result from the substitution of a nucleotide that is important for recognition of the tRNA by LeuRS. The G13:U22 pair within hs mt $tRNA^{Leu(UUR)}$ is highly conserved among eukaryotes (*7*); therefore, it appears reasonable that this set of nucleotides is contacted by the tRNA synthetase.

The trends observed with mutants of hs mt $tRNA^{Leu(UUR)}$ featuring alterations in the D stem highlight the importance of this domain in function. Subtle changes to the structure of this region effected by a subset of stabilizing mutations perturb both the conformation of the D loop and the reactivity with LeuRS. The D stem also appears to contain important aminoacylation determinants, as the introduction of a stabilizing mutation (U22C) (that does not negatively impact the structure of the hs mt $tRNA^{Leu(UUR)}$) attenuates aminoacylation.

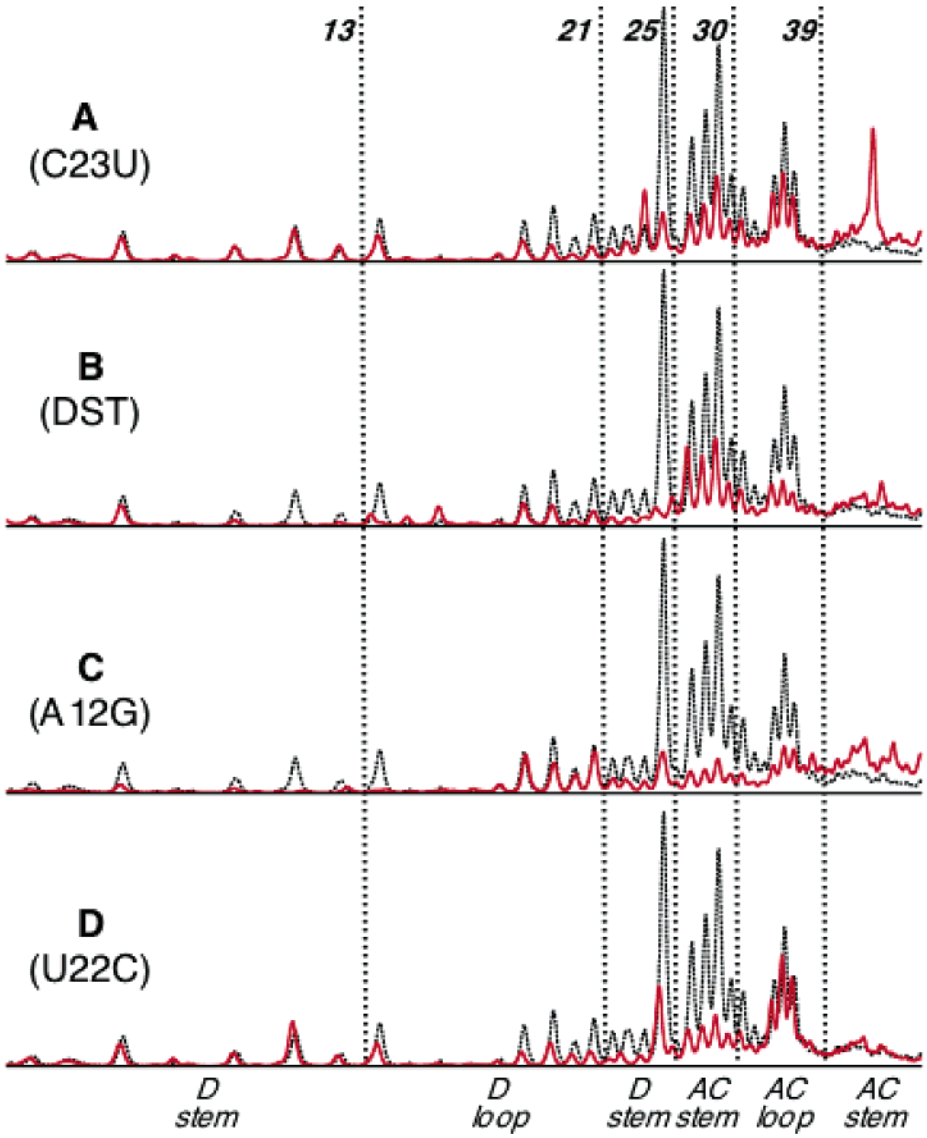

FIGURE 6: Histograms generated from cleavage data using S1 nuclease under native conditions (see Supporting Information for gel image). Results are exhibited in the same manner as in Figure 5.

Structural and Functional Effects of Mutations Stabilizing the Anticodon Stem of hs mt tRNA$^{Leu(UUR)}$. The anticodon stem of the WT tRNA$^{Leu(UUR)}$ exhibited significant susceptibility to nucleases specific for single-stranded RNA. To test the extent of denaturation within this stem, two mutants were compared to the WT tRNA. One contained a U40C mutation that introduces a CA mispair into the anticodon stem. This substitution corresponds to the U3271C mutation correlated with MELAS and MIDD (*28*, *29*). The behavior of this mutant was compared to a U40C/A30G construct containing an additional stabilizing mutation that restores the base pairing at the site of the pathogenic mutation and introduces a GC pair within the stem that is otherwise composed of AU pairs. Previous studies of these mutants indicate that the presence of the CA pair in the U40C mutant does attenuate aminoacylation and that the compensatory mutation restores activity (*11*). Chemical probing experiments indicated that the structure of the anticodon stem was disrupted by the destabilizing mutation and strengthened by the compensatory mutation relative to the WT tRNA$^{Leu(UUR)}$. Here, a more thorough investigation of global structural changes was undertaken using nuclease probing. In particular, the relationship between the structure of the anticodon stem and the D stem was analyzed.

Nuclease probing was performed on the U40C and U40C/A30G mutants, and the cleavage efficiencies were compared to those obtained with the WT hs mt tRNA$^{Leu(UUR)}$ (Figure 7). The general patterns of cleavage, particularly those obtained with RNase V1, were similar for the three tRNAs, indicating that the overall structures were similar. However, the extent of cleavage obtained with RNase T2 and nuclease S1 varied according to the stability of the anticodon stem, with the U40C mutant displaying higher susceptibility to these enzymes than the WT sequence or U40C/A30G mutant. The observation of increased cleavage at the stem nucleotides for the U40C mutant relative to WT hs mt tRNA$^{Leu(UUR)}$ confirms that this domain is at least partially structured for the WT tRNA. However, the decreased cleavage observed for the U40C/A30G mutant indicates that the WT anticodon stem is not well-ordered and that the GC pair installed by the set of mutations significantly enhances the structural integrity of the otherwise AU stem.

Interestingly, the amount of cleavage observed within the D stem is increased when the destabilizing U40C mutation

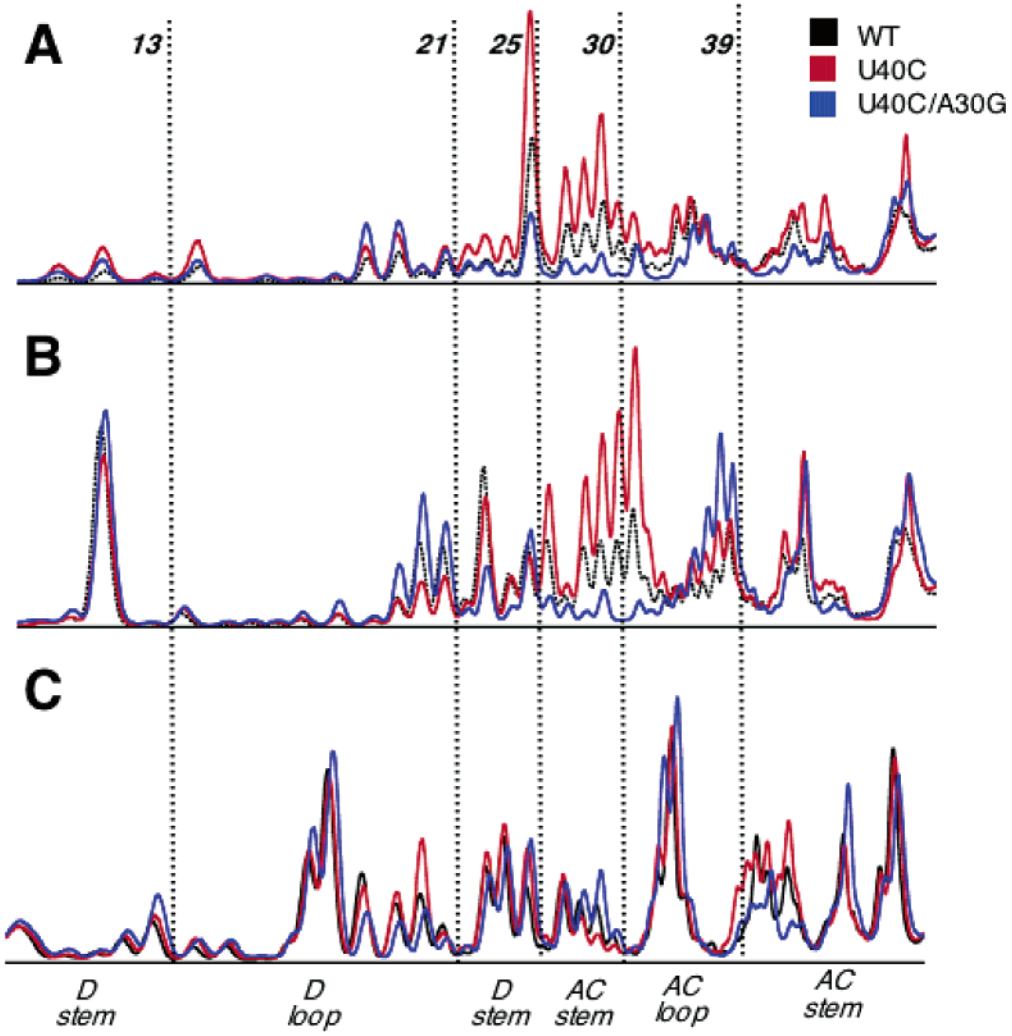

FIGURE 7: Histograms generated from cleavage data for enzymatic probing of WT tRNA$^{Leu(UUR)}$ and the U40C and U40C/A30G mutants (see Supporting Information for gel image). 5′-^{32}P-labeled tRNA was subjected to cleavage with nuclease S1, RNase T2, or RNase V1 and analyzed using 20% denaturing PAGE. Cleavage results were measured along each sample lane, and the data were used to create normalized histograms representing the cleavage patterns. (A) Nuclease S1 cleavage results for WT (black), U40C (red), and U40C/A30G (blue). The vertical lines represent boundaries of elements of secondary structure. Numbers to the left of each line represent the nucleotide terminating each domain. (B) Native RNase T2 cleavage results for WT (black), U40C (red), and U40C/A30G (blue). (C) Native RNase V1 probing data for WT (black), U40C (red), and U40C/A30G (blue).

is present, and cleavage of a subset of D stem nucleotides is decreased for the U40C/A30G mutant that features a stabilized anticodon stem (Figure 7). The anticodon mutants therefore mirror the behavior of the D stem mutants discussed above with the conformation of the D domain influenced by the conformation of the anticodon domain.

Contribution of Interdomain Communication to Effects of Pathogenic Mutations. It is apparent that there is significant interdomain communication between the anticodon and the D stems of hs mt tRNA$^{Leu(UUR)}$. The effects of pathogenic mutations within one domain may therefore be influenced by the weak structure of the other. This possibility was investigated by monitoring the aminoacylation of a mutant containing a pathogenic mutation and a D stem stabilized by the C23U mutation described above (Figure 8). Indeed, when the MELAS- and MIDD-related U40C (U3271C) substitution was tested within a U40C/C23U double mutant construct, the attenuated aminoacylation activity of the U40C mutant was restored to WT levels, indicating that the stabilizing mutation within the D stem strengthened the structure of the anticodon domain and made the tRNA less

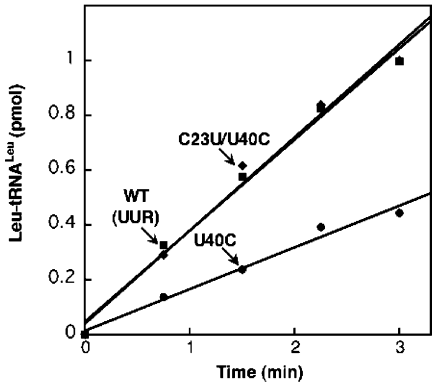

FIGURE 8: Aminoacylation activity for the C32U/U40C double mutant. The reactivity of WT hs mt tRNA$^{Leu(UUR)}$ (■), U40C (●), and C23U/U40C (♦) with conditions identical to Figure 4A.

susceptible to deactivation in the presence of the pathogenic mutation. The ability of a mutation in the D stem to rescue the functional activity of a mutant with a disrupted anticodon stem confirms that there is strong communication between the different domains of hs mt tRNA$^{Leu(UUR)}$. The stacking

interactions stabilizing the interface between the D and the anticodon stems may be highly sensitive to the integrity of base pairing within these domains, with dynamic defects existing in one stem propagated throughout the structure of this portion of the L-shaped tRNA structure.

The interdomain communication observed within the hs mt $tRNA^{Leu(UUR)}$ strongly parallels behavior documented in previous studies of hs mt $tRNA^{Ile}$ (*30*). Studies of this tRNA revealed that a structurally weak TΨC stem amplified the effects of pathogenic mutations in the anticodon stem. When a stabilizing mutation was introduced within the TΨC stem of hs mt $tRNA^{Ile}$, losses in aminoacylation caused by mutations within the anticodon stem were significantly less severe. In $tRNA^{Ile}$, therefore, structural defects are transmitted from one arm of the L-shaped tRNA tertiary fold to the other. It is apparent that weak structural elements within hs mt tRNAs promote functional defects in part because local instabilities are propagated throughout the entire structure.

CONCLUSIONS

The structure of hs mt $tRNA^{Leu(UUR)}$ contains unstable domains that are vulnerable to destabilizing mutations. The results reported here demonstrate that the D and anticodon stems of this tRNA are not rigidly structured, and moreover, suggest that the behavior of the two domains is strongly coupled, with the stability of one stem strongly influencing the structure of the other. Although the labile structure of hs mt $tRNA^{Leu(UUR)}$ appears to amplify the effects of disease-related mutations and therefore may play a role in resultant cellular effects, it appears that the flexibility of the structure is required for optimal function. Changes to the D stem that are strongly stabilizing appear to alter the structure of this stem and also decrease aminoacylation activity, indicating that the native fold requires the apparently dynamic structure. It appears that the unique structures of the hs mt tRNAs, although easily ruptured, contain idiosyncratic features required for function.

SUPPORTING INFORMATION AVAILABLE

Gel electrophoresis analysis of nuclease probing of tRNA mutants, native gel analysis of tRNA mutants, and thermal denaturation profiles. This material is available free of charge via the Internet at http://pubs.acs.org.

REFERENCES

1. Schimmel, P. (1979) in *Transfer RNA: Structure, Properties, and Recognition* (Schimmel, P., Söll, D., and Abelson, J., Eds.) pp 297−310, Cold Springs Harbor Laboratory Press, U.S.A.
2. Schon, E. A., Bonilla, E., and DiMauro, S. (1997) *J. Bioenerg. Biomembr. 29*, 131−149.
3. DiMauro, S., and Schon, E. A. (2001) *Am. J. Med. Genet. 106*, 18−26.
4. Wittenhagen, L. M., and Kelley, S. O. (2003) *Trends Biochem. Sci. 28*, 605−611.
5. Florentz, C., and Sissler, M. (2001) *EMBO Rep. 2*, 481−486.
6. Helm, M., Brule, H., Friede, D., Giegé, R., Putz, D., and Florentz, C. (2000) *RNA 6*, 1356−1379.
7. Sprinzl, M., Horn, C., Brown, M., Ioudovitch, A., and Steinberg, S. (1998) *Nucleic Acids Res. 26*, 148−153.
8. Gauss, D., Gruter, F., and Sprinzl, M. (1979) in *Transfer RNA: Structure, Properties and Function* (Schimmel, P., Söll, D., and Abelson, J., Eds.) pp 520−537, Cold Springs Harbor Laboratory Press, U.S.A.
9. MITOMAP: A Human Mitochondrial Genome Database (2000) Center for Molecular Medicine, Emory University, Atlanta, GA, http://www.mitomap.org/.
10. Wittenhagen, L. M., and Kelley, S. O. (2002) *Nat. Struct. Biol. 9*, 586−590.
11. Wittenhagen, L. M., Roy, M. D., and Kelley, S. O. (2003) *Nucleic Acids Res. 31*, 596−601.
12. Sohm, B., Frugier, M., Brule, H., Olszak, K., Przykorska, A., and Florentz, C. (2003) *J. Mol. Biol. 328*, 995−1010.
13. Park, H., Davidson, E., and King, M. P. (2003) *Biochemistry 42*, 958−964.
14. King, M. P., Koga, Y., Davidson, M., and Schon, E. A. (1992) *Mol. Cell. Biol. 12*, 480−490.
15. Jacobs, H. T., and Holt, I. J. (2000) *Hum. Mol. Genet. 9*, 463−465.
16. Flierl, A., Reichmann, H., and Seibel, P. (1997) *J. Biol. Chem. 272*, 27189−27196.
17. El Meziane, A., Lehtinen, S. K., Hance, N., Nijtmans, L. G., Dunbar, D., Holt, I. J., and Jacobs, H. T. (1998) *Nat. Genet. 18*, 350−353.
18. Zuker, M. (2003) *Nucleic Acids Res. 31*, 3406−3415.
19. Dirheimer, G., Keith, G., Dumas, P., and Westhof, E. (1995) in *tRNA Structure, Biosynthesis, and Function* (Söll, D., and RajBhandary, U., Eds.) pp 93−126, ASM Press, Washington, DC.
20. Oligo Extinction Coefficient Calculator (2000) The Scripps Research Institute, La Jolla, CA, http://www.scripps.edu/mb/gottesfeld/ExtCoeff.html.
21. Helm, M., Brule, H., Degoul, F., Cepanec, C., Leroux, J. P., Giegé, R., and Florentz, C. (1998) *Nucleic Acids Res. 26*, 1636−1643.
22. Bullard, J. M., Cai, Y. C., and Spremulli, L. L. (2000) *Biochim. Biophys. Acta 1490*, 245−258.
23. Shepard, A., Shiba, K., and Schimmel, P. (1992) *Proc. Natl. Acad. Sci. U.S.A. 89*, 9964−9968.
24. Suddath, F. L., Quigley, G. J., McPherson, A., Sneden, D., Kim, J. J., Kim, S. H., and Rich, A. (1974) *Nature 248*, 20−24.
25. Moras, D., Comarmond, M. B., Fischer, J., Weiss, R., Thierry, J. C., Ebel, J. P., and Giege, R. (1980) *Nature 288*, 669−674.
26. Shi, H., and Moore, P. B. (2000) *RNA 6*, 1091−1105.
27. Beuning, P. J., Tessmer, M. R., Baumann, C. G., Kallick, D. A., and Musier-Forsyth, K. (1999) *Anal. Biochem. 273*, 284−290.
28. Goto, Y., Nonaka, I., and Horai, S. (1991) *Biochim. Biophys. Acta 1097*, 238−240.
29. Tsukuda, K., Suzuki, Y., Kameoka, K., Osawa, N., Goto, Y., Katagiri, H., Asano, T., Yazaki, Y., and Oka, Y. (1997) *Diabetic Med. 14*, 1032−1037.
30. Kelley, S. O., Steinberg, S. V., and Schimmel, P. (2001) *J. Biol. Chem. 276*, 10607−10611.

BI035711Z